

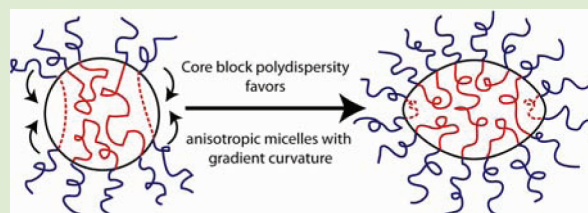
# Polydispersity-Driven Block Copolymer Amphiphile Self-Assembly into Prolate-Spheroid Micelles

Andrew L. Schmitt, Milton H. Repollet-Pedrosa, and Mahesh K. Mahanthappa\*

Department of Chemistry, University of Wisconsin-Madison, 1101 University Avenue, Madison, Wisconsin 53706, United States

**S** Supporting Information

**ABSTRACT:** The aqueous self-assembly behavior of polydisperse poly(ethylene oxide-*b*-1,4-butadiene-*b*-ethylene oxide) (OBO) macromolecular triblock amphiphiles is examined to discern the implications of continuous polydispersity in the hydrophobic block on the resulting aqueous micellar morphologies of otherwise monodisperse polymer surfactants. The chain length polydispersity and implicit composition polydispersity of these samples furnishes a distribution of preferred interfacial curvatures, resulting in dilute aqueous block copolymer dispersions exhibiting coexisting spherical and rod-like micelles with vesicles in a single sample with a O weight fraction,  $w_O$ , of 0.18. At higher  $w_O = 0.51$ – $0.68$ , the peak in the interfacial curvature distribution shifts and we observe the formation of only American football-shaped micelles. We rationalize the formation of these anisotropically shaped aggregates based on the intrinsic distribution of preferred curvatures adopted by the polydisperse copolymer amphiphiles and on the relief of core block chain stretching by chain-length-dependent intramicellar segregation.



Manipulating the micellar aggregate morphologies adopted by amphiphilic block copolymers (ABCs) in aqueous media is a fundamental problem in self-assembly, which has critical implications for the applications of these materials. Comprised of at least one hydrophobic segment covalently linked to a water-soluble polymer block, macromolecular amphiphiles self-assemble in water to form spherical and worm-like micelles and vesicles, depending on their overall degree of polymerization ( $N$ ) and their specific chemical compositions.<sup>1,2</sup> By virtue of their vanishingly small critical micelle concentrations, ABCs form persistent aggregates with more complex morphologies than their small-molecule congeners.<sup>3,4</sup> Persistent worm-like micelles and their branched variants are known to entangle in aqueous solutions, resulting in viscoelastic fluids useful in personal care products and in enhanced oil recovery.<sup>5–7</sup> Spherical micelles and vesicles (“polymersomes”) exhibit potential in the delivery of chemotherapeutics and peptide-based drugs, albeit with variable efficiencies.<sup>8,9</sup> Recent biological studies indicate that cells uptake high-aspect ratio particles more rapidly than spherical ones, which motivates the quest for ABCs that form persistent and nonspherical shapes as more effective drug delivery vehicles.<sup>10</sup> These examples illustrate the sensitive dependence of the physical properties of aqueous ABC dispersions and their applications on their self-assembly into micellar aggregates exhibiting well-defined shapes and sizes.

The search for new methods of controlling the micellar morphologies adopted by ABCs has profited immensely from the development of polymer syntheses that enable delicate tuning of the balance of noncovalent interactions that govern aqueous macromolecular assembly.<sup>11</sup> The preferred equilibrium morphology adopted by the simplest, monodisperse AB diblock or ABA triblock copolymer surfactants may be rationalized in

terms of Israelachvili’s critical packing parameter model, in which the equilibrium interfacial curvature of the micelle depends on the relative volumes filled by the hydrophobic block and the hydrated hydrophilic block. The micellar morphologies of monodisperse diblock and triblock copolymer surfactants are typically tuned by changing the polymer composition to change the packing constraints and preferred interfacial curvature. However, complex macromolecular architectures such as Janus-type dendritic amphiphiles assemble into more complex structures, including tubules, helical ribbons and fibrils, and even cube-shaped micelles.<sup>12–14</sup> The groups of Manners, Winnik, and Hillmyer have recently exploited hydrophobic core block crystallization as a means of tuning the self-assembly of rod-like micelles in narrow dispersity block copolymers.<sup>15–17</sup> Liquid crystallinity in the hydrophobic core block has also been employed as a means of controlling and dynamically switching noncovalent assemblies of polymeric micelles.<sup>18,19</sup> Because these approaches to complex micellar morphologies require the execution of complex, multistep chemical syntheses, simpler methods for manipulating the micellar morphologies formed by commodity ABCs are desirable.

The use of block polydispersity as a tool for manipulating the micellar morphologies of ABCs in aqueous media remains relatively unstudied. Using a mixture of block copolymers, where each component exhibits a different preferential curvature, enables formation of morphologies exhibiting nonconstant interfacial mean curvatures. To the best of our

**Received:** November 7, 2011

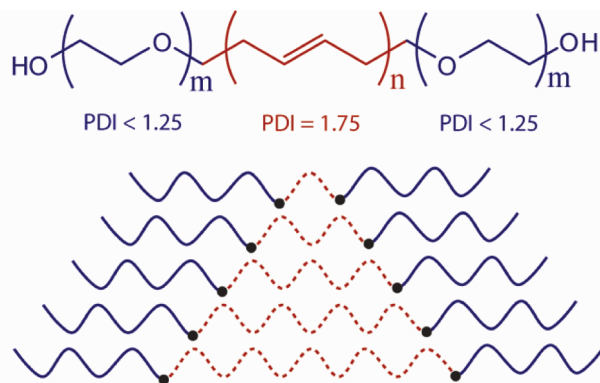
**Accepted:** January 19, 2012

**Published:** January 25, 2012

knowledge, only a few reports have carefully considered the effects of *discrete polydispersity* in ABC self-assembly by examining the morphological behavior of blends of monodisperse ABCs.<sup>3,20–22</sup> Recently, we and others have demonstrated that the selective incorporation of *continuously polydisperse* segments into block copolymers provides new opportunities to subtly tune the interfacial curvatures of melt microphase separated block copolymer morphologies and to access nonconstant mean curvature structures.<sup>23–25</sup> Herein, we extend this concept to ABC self-assembly to demonstrate the unique consequences of continuous polydispersity on the dilute aqueous solution behavior of polydisperse triblock amphiphiles comprised of a polydisperse hydrophobic block flanked by narrow dispersity water-soluble segments.

We recently reported the synthesis and molecular characterization of a series of polydisperse OBO triblock copolymers (O = poly(ethylene) oxide; B = perfectly regioregular poly(1,4-butadiene)), in which the center B block has broad polydispersity and the O end blocks have relatively narrow dispersities (Scheme 1).<sup>26</sup> These materials were synthesized by

**Scheme 1. Poly(ethylene oxide-*b*-1,4-butadiene-*b*-ethylene oxide) (OBO) Triblock Copolymers with Broad and Continuous Middle Block Polydispersity**



tandem chain-transfer ring-opening metathesis polymerizations (ROMP-CT) of 1,5,9-cyclododecatriene and anionic ring-opening polymerizations of ethylene oxide. By polymer degradation analyses, we showed that the O end blocks have  $M_w/M_n \leq 1.25$ ; whereas, the center B blocks exhibit a broad continuous polydispersity,  $M_w/M_n = 1.74$ .<sup>26</sup> The molecular characteristics of four polydisperse OBO triblocks and two monodisperse mOBO triblocks (derived from tandem anionic polymerizations) are provided in Table 1 (see Supporting Information, Table S1, for detailed molecular characterization). Aqueous dispersions of these polymers were produced by dropwise addition of deionized water to a rapidly stirred 10 wt % polymer solution in tetrahydrofuran (THF) to yield a final solution containing 1 wt % polymer. This solution was then dialyzed against deionized water for 7–10 days to affect complete solvent exchange. We selected the induced-micellization method of adding a selective solvent to a polymer solution in a nonselective solvent based on prior literature, which suggests that this method facilitates the formation of equilibrium structures.<sup>27–29</sup>

We investigated the dilute solution morphologies of OBO-w18 (O weight fraction  $w_O = 0.18$ ) and OBO-w24 ( $w_O = 0.24$ ) using a combination of cryogenic transmission electron microscopy (cryoTEM) and dynamic light scattering (DLS).

**Table 1. Molecular Characterization of Polydisperse OBO Triblock Amphiphiles and Their Aqueous Solution Morphologies**

sample	$w_O^a$	$N_B^a$	PDI $B^a$	$R_h^b$ (nm)	PI <sup>b</sup>	solution <sup>d</sup>
OBO-w58	0.58	153	1.74	$35 \pm 1$	0.3	spheroid
OBO-w42	0.42	153	1.74	$31 \pm 2$	0.4	spheroid
OBO-w24	0.24	153	1.74	$43 \pm 11$	$11 \pm 2^c$	B, C, S
OBO-w18	0.18	187	1.75	$34 \pm 8$	$3 \pm 2^c$	B, C, S
mOBO-w68	0.68	170	1.06	$16 \pm 0.3$	0.3	S
mOBO-w51	0.51	170	1.06	$18 \pm 0.1$	0.5	S

<sup>a</sup>Complete molecular characteristics can be found in Supporting Information, Table S1. <sup>b</sup>Determined from DLS. <sup>c</sup>Values for the bimodal size distribution derive from DLS data analyses that assume the presence of two or more populations of hard sphere, point scatterers. <sup>d</sup>Determined from cryoTEM images (B = bilayer vesicles, C = cylinders, and S = spheres).

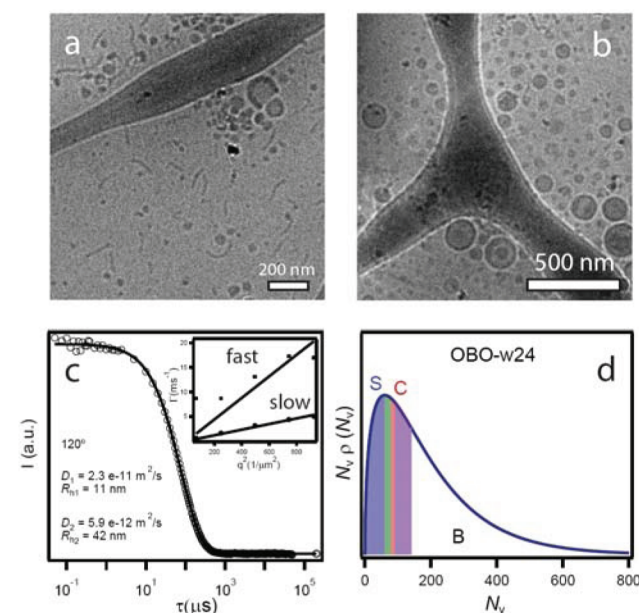


**Figure 1.** Cryo-TEM images of vitrified aqueous 1 wt % solutions of (a) OBO-w18 and (b) OBO-w24. Panel (c) shows the autocorrelation function obtained from dynamic light scattering on a 1 wt % solution of OBO-80 at 22 °C using 120°-angle detection and the accompanying best fit to a double exponential function assuming the presence of at least two populations of hard sphere point scatterers (inset shows fitting the slow and fast relaxation delays). Panel (d) shows the number density of chains having a given  $N_{v,tot}$  weighted by  $N_{v,tot}$  where molecules with small  $N_{v,tot}$  correspond to chains with high  $w_O$ . The resulting preferred curvatures are calculated based on behavior of model OB diblocks (see SI for more details), where the blue region prefers spheres (S), red is cylinders (C), unfilled is bilayer vesicles (B), green is S + C coexistence, and purple is C + B coexistence.

Specimens for cryoTEM imaging were prepared by vitrification of thin aqueous films on copper TEM grids in liquid ethane ( $-80$  °C).<sup>30</sup> Representative cryoTEM images of OBO-w18 and OBO-w24 demonstrate that these polydisperse amphiphiles form arrays of coexisting spheres, short rods, and vesicles (Figure 1a,b). As a consequence of this coexistence of morphologies with varying sizes and shapes, single exponential decay functions fail to adequately fit the autocorrelation function observed by DLS, even upon using a cumulant expansion that incorporates an aggregate size polydispersity

index (PI). The data can be more reasonably described by the double exponential decay fit shown in Figure 1c. However, this analysis assumes the presence of two or more populations of hard sphere point scatterers and ignores the coexistence of different micellar morphologies and their various scattering contributions (see Supporting Information for details).

While the average chemical compositions of these samples sit in a range where one might expect to observe vesicles, the chain length polydispersity in only the center block imposes both composition and chain length polydispersities on the overall block copolymer sample. Since each O block is monodisperse, longer copolymer chains have larger B blocks, lower  $w_O$ , and different interfacial curvatures (Scheme 1) as compared to the shorter O-rich chains. Therefore, polymer chains in these samples exhibit a broad distribution of preferred interfacial curvatures. Using the molecular weight distributions of each block in OBO-w24, we have plotted the weight fraction of chains as a function of the volume degree of polymerization,  $N_{v,tot}$  of the chain in Figure 1d (see Supporting Information for detailed calculations). Using the known morphology diagram for narrow dispersity OB diblock copolymers,<sup>4</sup> we have marked the polymer composition cut-offs that correspond to spheres, worms, and vesicles to show the distribution of interfacial curvatures present in the sample. This analysis clearly shows that OBO-w24 contains a large fraction of chains that favor vesicle formation, with significant populations that prefer to form spheres and worms (Figure 1d). On these grounds, multiple phase coexistence should be anticipated in ABCs with polydisperse hydrophobic core blocks. In the induced micellization protocol, kinetic trapping of shorter chains in an aggregate comprised of primarily larger chains results in the formation new and unusual structures, which exhibit both high curvature interfaces reminiscent of spheres and flat-curvature interfaces akin to that of vesicles. Therefore, presence of a substantial number of sphere-forming copolymers in the distribution translates into the formation of short rod-like micelles and unusual cup-like vesicles. This phenomenon is related to the recently reported budding and break-up of worm-like micelles by virtue of core block degradation in poly( $\epsilon$ -caprolactone-*b*-ethylene oxide) diblock copolymers.<sup>31</sup>

In contrast to the variety of morphologies observed in OBO-w18 and OBO-w24, aqueous dispersions of OBO-w42 and OBO-w58 exhibit very different behavior. Based on the average chemical composition of these polymers ascertained by <sup>1</sup>H NMR spectroscopy, monodisperse polymers at these compositions would be expected to exhibit a spherical micelle morphology. However, these polydisperse ABC dispersions form prolate spheroidal micelles with tapered ends similar in shape to American footballs (Figure 2a,b). From image analyses of 10 individual micelles, the footballs formed by OBO-w48 have a major axis measuring 36 nm with an aspect ratio of  $\sim 1.4$ . This result concurs with single-exponential fits of the DLS data from which the micellar hydrodynamic radius is  $R_H = 31$  nm (polydispersity (PI)  $\leq 0.5$ ), assuming a perfectly spherical particle (Figure 2c). Increasing the O content as in OBO-w58 results in a lengthening of the major axis to 40 nm with a similar aspect ratio  $\sim 1.5$ ; DLS studies again confirm a unimodal distribution of roughly spherical objects with  $R_H = 35$  nm (PI  $\leq 0.5$ ). The anisotropy of the spheroids accounts for the difference between the micellar radius determined by DLS and cryoTEM.<sup>32</sup> While cryoTEM provides only a two-dimensional image of the American football-shaped aggregates, we can rule out the possibility that these micelles are oblate

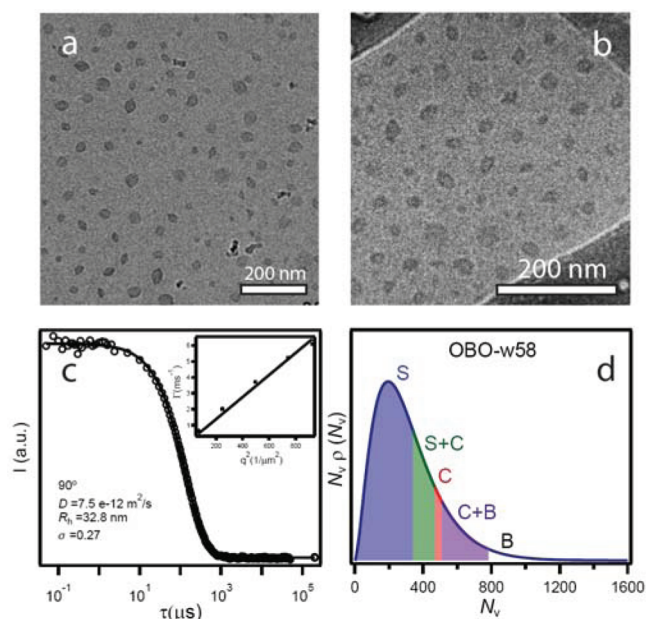


**Figure 2.** Cryo-TEM images of vitrified aqueous 1 wt % solutions of (a) OBO-w42 and (b) OBO-w58. Panel (c) shows the dynamic light scattering autocorrelation functions obtained from a 1 wt % solution of OBO-w58 at room temperature using 90°-angle detection fit with a single exponential function with cumulant expansion (inset shows a fit of relaxation delay as a function of  $q^2$ ). Panel (d) shows the number density of chains having a given  $N_{v,tot}$  weighted by  $N_{v,tot}$  where molecules with small  $N_{v,tot}$  correspond to chains with high  $w_O$ . The preferred interfacial curvatures are calculated based on model behavior (see Supporting Information for more details) where the blue region prefers spheres (S), red is cylinders (C), unfilled is bilayer vesicles (B), green S + C coexistence, and purple is coexisting C and B.

disks. It is highly unlikely that all of the micelles would be oriented sideways in every TEM image. Even if shear forces due to sample blotting perturb the preferred orientation of the micelles with respect to the imaging plane, the relaxation delay used in the vitrification process ( $\sim 15$  s) should allow for orientational relaxation of our anisotropic aggregates. We also note that monodisperse polymer amphiphiles mOBO-w51 and mOBO-w68 form spherical micelles with  $R_H = 18$  and 16 nm, respectively (see Supporting Information, Figures S1(a) and S3, respectively). Note that these radii are only half of that observed for the polydisperse OBO-w58 or OBO-w42. Therefore, we conclude that chain length polydispersity drives the formation of football-shape micelles whose dimensions are governed primarily by the long chains in the molecular weight distribution of the core B block.

To corroborate the formation of nonspherical micellar aggregates, we performed high-resolution synchrotron small-angle X-ray scattering on 5 wt % aqueous dispersions of our polydisperse OBO materials and analyzed the scattering profiles using several known models (see Supporting Information, Figures S2–S4). Core–shell sphere models capture the behavior of sphere-forming monodisperse mOBO-w68 (Figure S2). However, attempts to analyze synchrotron SAXS profiles derived from polydisperse OBO-w42 with this model yield poor quality fits that suggest the nonspherical nature of these aggregates (Figure S3). Slightly better fits for OBO-w42 were obtained using a core–shell cylinder with a micellar aspect ratio of 1.2 (Figure S4). More complex models are likely necessary to capture the unusual form-factor scattering from these micellar

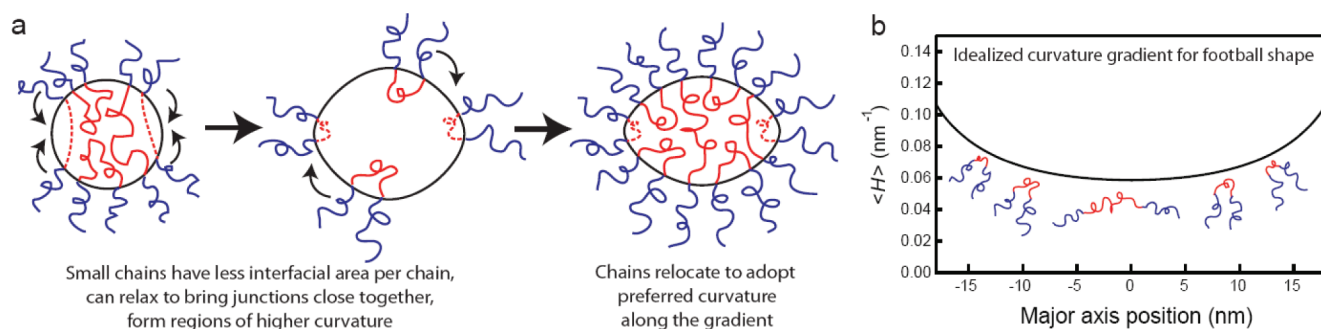


**Figure 3.** (a) Schematic representation of polydispersity-induced self-assembly of American football-shaped micelles. Chain length-dependent intramicellar segregation is driven by the relaxation of short chain stretching that induces a gradient in the interfacial curvature within the aggregate along the major axis of the prolate spheroid. (b) Calculated mean curvature along the major axis ( $a = 18$  nm) of an idealized football-shaped micelle based on OBO-w42 emphasizing the distribution in mean curvatures along the micelle surface (details of this the calculation are provided in the Supporting Information).

aggregates. For systems with low X-ray scattering contrast and complex morphologies such as the ones presented here, cryoTEM is a much more valuable characterization tool. A collage of cryoTEM images from prolate-spheroid forming copolymers is provided in Figure S7.

In view of recent work implicating core block crystallinity as a driving force for formation of anisotropically shaped micellar aggregates,<sup>15–17</sup> we studied the thermal properties of our OBO triblock copolymers to assess the relevance of such effects. The ROMP-CT synthesis of the polydisperse core B block yields a perfectly regioregular poly(1,4-butadiene) with  $\sim 80\%$  *trans*-double bonds, resulting in a low level of crystallinity.<sup>33</sup> Differential scanning calorimetry (DSC) analysis of OBO-w42 in the absence of water reveals a B block melting temperature  $T_{m,B} = 41$  °C and  $T_{m,O} = 57$  °C for the O block (see Supporting Information, Figure S2). Using the theoretical heat of fusion for perfectly crystalline *trans*-poly(1,4-butadiene) homopolymer,<sup>34</sup> we find that the B block exhibits 8.3 wt % crystallinity. Upon induced micellization to form a 1 wt % OBO-w42 solution in water, DSC analyses of the aqueous copolymer dispersions show that the B block melting temperature drops to 38 °C with an accompanying drop in the crystallinity to 4.4 wt %, consistent with expectations for polymer crystallization in nanoconfinement.<sup>35</sup> Based on Yin and Hillmyer's work implicating crystallinity in the formation of anisotropic micellar morphologies in which the core crystallinity is typically greater than  $\sim 30\%$ ,<sup>17</sup> we speculate that the low level of crystallinity in the B core block does not contribute appreciably to the formation of anisotropic micellar aggregates by polydisperse OBO amphiphiles.

Instead, we hypothesize that the polydispersity in both composition and chain length implied by the continuous polydispersity of the center B block in OBO triblock copolymers (Scheme 1) drives the formation of American football-shaped micelles. The compositions of most of the OBO chains in OBO-w58 and OBO-w42 are within the expected spherical micelle window for monodisperse amphiphiles (Figure 2d). The B block polydispersity translates into a chain length-dependent preference to form spheres of different sizes, by virtue of the different interfacial area requirements per chain. Chains with smaller B blocks consequently prefer to form higher curvature and thus smaller spheres, whereas those with larger B blocks form larger spheres with flatter interfaces. If these polydisperse chains remain completely mixed within a single spherical micelle with constant mean curvature, the

broad distribution of interfacial areas per chain would cause the short chains to stretch in an entropically unfavorable manner. We hypothesize that this unfavorable entropy of short chain stretching overrides the configurational entropy gain associated with chain mixing within the micelle, thus driving chain length-dependent intramicellar segregation based on preferred interfacial curvature (Figure 3a). A similar effect has been predicted in continuously polydisperse vesicle-forming diblocks, where shorter chains segregate to the inner bilayer and longer chains segregate to the slightly flatter outer bilayer.<sup>36</sup> The OBO triblock architecture may enhance the propensity for chain length segregation, since the local concentration of short chains is increased due to the topological constraints of the triblock architecture. By this mechanism, the curvature gradient of the football-shaped micelles reflects the specific chain length distribution in the polydisperse OBO samples that we have synthesized (Figure 3b).

These preliminary results on the dilute solution self-assembly of polydisperse OBO triblock copolymer surfactants demonstrate that polydispersity represents a composition and molecular weight-independent means of manipulating the observed micellar morphologies. Polydisperse OBO triblock copolymers at low  $w_O$  form coexisting vesicle, rod-like, and spherical micelles by virtue of the composition polydispersity arising from polydispersity in the hydrophobic core B block. When a majority of the chains exhibit compositions that favor the formation of spherical micelles, hydrophobic block polydispersity and the consequent compositional polydispersity drive intramicellar chain segregation to form tapered football-shaped micelles. Thus continuous polydispersity in block copolymer amphiphiles presents a new opportunity for morphological control that may have important consequences for future applications of these materials.

## ■ ASSOCIATED CONTENT

### 📄 Supporting Information

Detailed molecular characterization of triblock copolymers, micellar dispersion preparation, dynamic light scattering data collection and modeling, synchrotron small-angle X-ray scattering, differential scanning calorimetry, cryoTEM sample preparation, and cryoTEM of mOBO-51, addition cryoTEM images of American footballs, analysis of the composition polydispersity, and details of the curvature calculation in Figure 3b. This material is available free of charge via the Internet at <http://pubs.acs.org>.

## ■ AUTHOR INFORMATION

## Corresponding Author

\*E-mail: mahesh@chem.wisc.edu. Tel.: +1 (608) 262-0421.

## Notes

The authors declare no competing financial interest.

## ■ ACKNOWLEDGMENTS

A.L.S. gratefully acknowledges financial support from a NSF American Competitiveness in Chemistry Postdoctoral Fellowship (CHE-1041975). M.K.M gratefully acknowledges financial support from an NSF CAREER Award (DMR-0748503) and the Donors of the American Chemical Society Petroleum Research Fund (ACS PRF 47143-G7). This research was further supported by the NSF Materials Research Facilities Network grant and relied on use of NSF MRSEC/NSEC core characterization facilities at UW–Madison (DMR-0520527 and DMR-0425880) and the NSF-funded Institute of Technology Characterization Facility at the University of Minnesota (DMR-0212302 and DMR-0819885). We thank Professor Nicholas Abbott for use of his dynamic light scattering apparatus. SAXS experiments were performed at the DuPont–Northwestern–Dow Collaborative Access Team (DND-CAT) located at Sector 5 of the Advanced Photon Source (APS). DND-CAT is supported by E.I. DuPont de Nemours and Co., The Dow Chemical Company and Northwestern University. Use of the APS, an Office of Science User Facility operated for the U.S. Department of Energy (DOE) Office of Science by Argonne National Laboratory, is supported by the U.S. DOE under Contract No. DE-AC02-06CH11357.

## ■ REFERENCES

- (1) Hillmyer, M. A. *Science* **2007**, *317*, 604–605.
- (2) Discher, D. E.; Eisenberg, A. *Science* **2002**, *297*, 967–973.
- (3) Jain, S.; Bates, F. S. *Macromolecules* **2004**, *37*, 1511–1523.
- (4) Jain, S.; Bates, F. S. *Science* **2003**, *300*, 460–464.
- (5) Walker, L. M. *Curr. Opin. Colloid Interface Sci.* **2001**, *6*, 451–456.
- (6) Won, Y.-Y.; Bates, F. S. *Surfactant Sci. Ser.* **2007**, *140*, 417–451.
- (7) Daripa, P.; Pasa, G. *Int. J. Eng. Sci.* **2004**, *42*, 2029–2039.
- (8) Discher, B. M.; Won, Y.-Y.; Ege, D. S.; Lee, J. C. M.; Bates, F. S.; Discher, D. E.; Hammer, D. A. *Science* **1999**, *284*, 1143–1146.
- (9) Bromberg, L. J. *Controlled Release* **2008**, *128*, 99–112.
- (10) Gratton, S. E. A.; Ropp, P. A.; Pohlhaus, P. D.; Luft, J. C.; Madden, V. J.; Napier, M. E.; DeSimone, J. M. *Proc. Natl. Acad. Sci. U.S.A.* **2008**, *105*, 11613–11618.
- (11) Holder, S. J.; Sommerdijk, N. A. J. M. *Polym. Chem.* **2011**, *2*, 1018–1028.
- (12) Percec, V.; Wilson, D. A.; Leowanawat, P.; Wilson, C. J.; Hughes, A. D.; Kaucher, M. S.; Hammer, D. A.; Levine, D. H.; Kim, A. J.; Bates, F. S.; Davis, K. P.; Lodge, T. P.; Klein, M. L.; De, V. R. H.; Aqad, E.; Rosen, B. M.; Argintaru, A. O.; Sienkowska, M. J.; Rissanen, K.; Nummelin, S.; Ropponen, J. *Science* **2010**, *328*, 1009–1014.
- (13) Cho, B.-K.; Jain, A.; Gruner, S. M.; Wiesner, U. *Chem. Commun.* **2005**, 2143–2145.
- (14) del, B. J.; Oriol, L.; Sanchez, C.; Serrano, J. L.; Di, C. A.; Keller, P.; Li, M.-H. *J. Am. Chem. Soc.* **2010**, *132*, 3762–3769.
- (15) Gaedt, T.; Jeong, N. S.; Cambridge, G.; Winnik, M. A.; Manners, I. *Nat. Mater.* **2009**, *8*, 144–150.
- (16) Presa, S. A.; Gilroy, J. B.; Winnik, M. A.; Manners, I. *Angew. Chem., Int. Ed.* **2010**, *49*, 8220–8223, S8220/1–19.
- (17) Yin, L.; Hillmyer, M. A. *Macromolecules* **2011**, *44*, 3021–3028.
- (18) Bae, J.; Choi, J.-H.; Yoo, Y.-S.; Oh, N.-K.; Kim, B.-S.; Lee, M. J. *Am. Chem. Soc.* **2005**, *127*, 9668–9669.
- (19) Kim, H.; Jeong, S.-M.; Park, J.-W. *J. Am. Chem. Soc.* **2011**, *133*, 5206–5209.
- (20) Terreau, O.; Luo, L.; Eisenberg, A. *Langmuir* **2003**, *19*, 5601–5607.
- (21) Terreau, O.; Bartels, C.; Eisenberg, A. *Langmuir* **2004**, *20*, 637–645.
- (22) Zhou, D.; Alexandridis, P.; Khan, A. J. *Colloid Interface Sci.* **1996**, *183*, 339–350.
- (23) Widin, J. M.; Schmitt, A. K.; Im, K.; Schmitt, A. L.; Mahanthappa, M. K. *Macromolecules* **2010**, *43*, 7913–7915.
- (24) Lynd, N. A.; Hillmyer, M. A. *Macromolecules* **2005**, *38*, 8803–8810.
- (25) Widin, J. M.; Schmitt, A. K.; Im, K.; Schmitt, A. L.; Mahanthappa, M. K. *J. Am. Chem. Soc.* **2012**, DOI: 10.1021/JA210548E.
- (26) Schmitt, A. L.; Mahanthappa, M. K. *Soft Matter* **2011**, DOI: 10.1039/C2SM07041C.
- (27) Zhang, L.; Yu, K.; Eisenberg, A. *Science* **1996**, *272*, 1777–1779.
- (28) Moffitt, M.; Khougaz, K.; Eisenberg, A. *Acc. Chem. Res.* **1996**, *29*, 95–102.
- (29) Meli, L.; Lodge, T. P. *Macromolecules* **2009**, *42*, 580–583.
- (30) Cui, H.; Hodgdon, T. K.; Kaler, E. W.; Abezgauz, L.; Danino, D.; Lubovsky, M.; Talmon, Y.; Pochan, D. J. *Soft Matter* **2007**, *3*, 945–955.
- (31) Loverde, S. M.; Ortiz, V.; Kamien, R. D.; Klein, M. L.; Discher, D. E. *Soft Matter* **2010**, *6*, 1419–1425.
- (32) Bhalla, G.; Deen, W. M. J. *J. Membr. Sci.* **2007**, *306*, 116–124.
- (33) Bielawski, C. W.; Grubbs, R. H. *Angew. Chem., Int. Ed.* **2000**, *39*, 2903–2906.
- (34) *Polymer Data Handbook*, 2nd ed.; Oxford University Press: New York, 2009.
- (35) Weimann, P. A.; Hajduk, D. A.; Chu, C.; Chaffin, K. A.; Brodil, J. C.; Bates, F. S. *J. Polym. Sci., Polym. Phys.* **1999**, *37*, 2053–2068.
- (36) Jiang, Y.; Chen, T.; Ye, F.; Liang, H.; Shi, A.-C. *Macromolecules* **2005**, *38*, 6710–6717.